J Mater Sci (2011) 46:55–62
DOI 10.1007/s10853-010-4795-7

Effect of inversion on thermoelastic and thermal transport properties of $MgAl_2O_4$ spinel by atomistic simulation

P. Shukla · A. Chernatynskiy · J. C. Nino · S. B. Sinnott · S. R. Phillpot

Received: 20 February 2010 / Accepted: 24 July 2010 / Published online: 11 August 2010

Abstract $MgAl_2O_4$ is commonly found in the normal spinel structure with the Mg^{2+} ions located in tetrahedral sites and the Al^{3+} ions occupying octahedral sites. We use atomic-level simulation to characterize the effect of inversion on the elastic and thermal properties. Cation ordering and volumetric changes tend to affect the structure and properties in opposite ways, thereby compensating each other up for up to 50% inversion. For higher inversions, volumetric effects dominate. In the case of the thermal conductivity, the effects of changes in the elastic properties and thermal expansion essentially cancel over the entire range of inversion.

Introduction

Oxide spinels are versatile compounds that are used in electrical, optical, mechanical, and magnetic applications [1]. For example, $MgIn_2O_4$ is a promising transparent electronic conductor [2], while $MgAl_2O_4$ has been proposed as a matrix for the storage of radioactive waste generated in the nuclear fuel cycle [3]. $MgAl_2O_4$ has also been proposed as a possible component of an inert matrix fuel (IMF) system [4, 5]. Key performance metrics of IMF systems include good radiation tolerance and high thermal conductivity. Spinels are known to be very radiation resistant and their mechanical properties are also robust under irradiation [6, 7]. This radiation resistance, particularly of $MgAl_2O_4$, has been attributed to both a high interstitial-vacancy recombination rate [8] and to the ease with which they tolerate cation anti-site disorder while still maintaining crystallinity [9, 10]. It is therefore of significant interest to gain a better understanding of inversion and to characterize the elastic, thermal expansion and thermal transport properties of spinel-structured oxides as a function of the anti-site disorder, or inversion.

Spinels belong to space group $Fd\bar{3}m$ (No. 227). The general formula for the spinel compounds is AB_2O_4, where A is usually a divalent cation and B is a trivalent cation. In our case, A is Mg^{2+} and sits on 8a tetrahedral sites, while B is Al^{3+} and occupies the 16b octahedral sites. The cubic unit cell thus contains eight formula units for a total of 56 ions. This unit cell can be considered as consisting of eight cubic subunits as shown in Fig. 1. In the fully inverted structure, all the occupied tetrahedral sites contain B ions, while one half of the octahedral sites contain A ions; the other half are occupied by B ions. For an excellent review on the spinel structure the reader is referred to the paper by Sickafus et al. [11].

For AB_2O_4, inversion involves the exchange of A and B ions and is quantified as the ratio of the number of A cations sitting on B sites to the total number of A ions in the system. Different spinel-structured materials exhibit different degrees of inversion, depending upon the cation radius ratio and their charges [8]. To elucidate the effect of inversion on elastic and thermal properties, it is desirable to scrutinize the system over the full range of inversion. However, there is no single spinel material that experimentally spans the whole range of inversion from normal ($i = 0$) to completely inverted ($i = 1$). For example, natural $MgAl_2O_4$, which has been equilibrated over geological times in the Earth's crust, has an inversion value close to 0 [10]; however, synthetic samples exist over the range of $i \sim 0.1$–0.3, with the degree of inversion depending on the

P. Shukla · A. Chernatynskiy · J. C. Nino · S. B. Sinnott · S. R. Phillpot (✉)
Department of Materials Science and Engineering, University of Florida, Gainesville, FL 32611, USA
e-mail: sphil@mse.ufl.edu

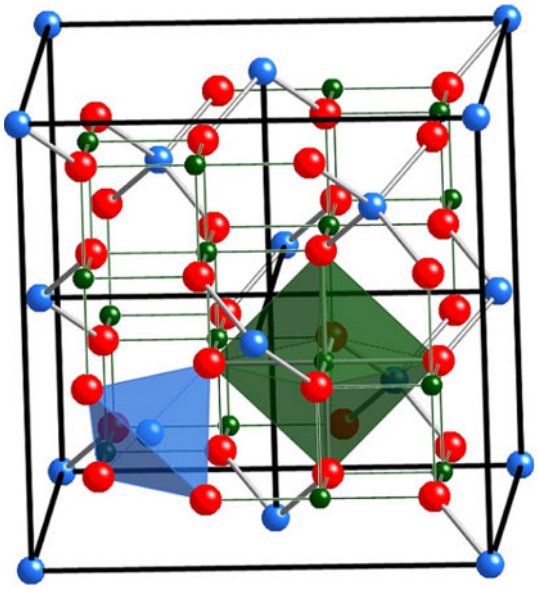

Fig. 1 Cubic spinel unit cell with Mg (*blue*, *medium* sized), Al (*green*, *small*) and O (*red*, *large*) atoms. The unit cell is divided into eight subunits with Mg tetrahedral (*blue*) and Al octahedral (*green*) in alternating sub-cells (Color figure online)

synthesis process [12]. To achieve $i \sim 0.3$ a sample has to anneal for a few minutes at sufficiently high temperature [13, 14]. Higher degrees of inversion ($i \sim 0.6$–0.7) can also be achieved by neutron irradiation [8]. By contrast, $MgGa_2O_4$ is typically found with $i \sim 0.5$, while $MgIn_2O_4$ is generally fully inverse ($i \sim 1.0$) [15].

Since no single system manifests the full range of inversion, in systematically characterizing the properties it is difficult to decouple the effects of inversion from those of changing the composition of the system. Atomic-level calculations and simulations provide the ideal vehicle to separate these effects. Therefore, in this article we characterize the structure, elastic properties, thermal expansion, and thermal conductivity of a single spinel system over the full range of inversion from $i = 0$ to $i = 1$. We focus on $MgAl_2O_4$ as a suitable model material.

Andreozzi et al. [12] reported the effect of temperature on cation ordering in $MgAl_2O_4$ and concluded that inversion increases from $i = 0.18$ to $i = 0.29$ between 600 and 1,100 °C. Suzuki et al. [16] reported a transition temperature ($T_c \sim 627$ °C), around which thermal expansion and bulk modulus show discontinuities. They also reported a change in the Grüneisen parameter around T_c. In addition, Suzuki and Kumazawa [17] reported a change in the coefficient of thermal expansion with temperature. However, no experimental study has been able to unequivocally separate the effects of temperature from inversion because temperature largely determines the inversion.

As previously noted, calculations and simulations are ideal tools to elucidate the effect of inversion. Density functional theory (DFT) and Monte Carlo (MC), along with molecular dynamics (MD), have been used to investigate the effect of inversion on $MgAl_2O_4$. For instance, Ball et al. [10] used MD to show that the lattice parameter decreases with inversion in $MgAl_2O_4$. Consistent with this study and also with experiment, DFT calculations by Seko et al. [18] found that inversion leads to an increase in density. Using MC, Lavrentiev et al. [19] found that the degree of inversion increases with temperature. Another MC simulations by Seko et al. [18] also reported that the degree of inversion depends on temperature. Thibaudeau and Debernardi [20] used DFT perturbation theory to determine the phonon spectra of normal $MgAl_2O_4$ and calculated the Grüneisen parameter, which matched well with experiment. The only simulation work that investigated the effect over the entire range of inversion was by Li et al. [21], who showed how cation ordering affects the mechanical properties, but provided no explanation for the observed behavior. In this article, we have extended the study of Li et al. [21], by also characterizing the thermal transport properties. One of the key performance metrics of candidate IMF materials is the thermal conductivity, which should be at least as high as that of UO_2, the currently used nuclear fuel [22]. The degree of inversion of $MgAl_2O_4$ increases under irradiation. However, the effect of this inversion on thermal conductivity has not yet been determined: we do so here.

Simulation methodology

The ions in spinel are modeled as point masses that initially sit at crystal sites with formal charges ($q_{Mg} = +2$, $q_{Al} = +3$, $q_O = -2$). The interactions between the ions are described by the Coulomb potential supplemented by a standard Buckingham potential [23] for the short-ranged (up to 16 Å), mainly repulsive interaction:

$$E_{ij} = \frac{1}{4\pi\varepsilon_0}\frac{q_i q_j}{r_{ij}} + \left[A_{ij}\exp\left(\frac{-r_{ij}}{\rho_{ij}}\right) - \frac{C_{ij}}{r_{ij}^6}\right] \quad (1)$$

The Buckingham potential is described by three parameters: A, ρ, and C for each species pair. For these simulations the parameters are taken from Ball et al. [10] and are shown in Table 1.

There are various numerical techniques that effectively compute the Coulomb energy; we use the charge neutralized direct summation method [24] because of its computational efficiency.

The elastic properties of normal $MgAl_2O_4$ were calculated and compared with DFT calculations and experiment [21, 25] (see Table 2). Other experimental studies have also reported similar values [16, 26, 27]. It is evident that the elastic constants and moduli calculated with the potential

Table 1 Buckingham potential parameters (Mg and Al interact only via Coulombic repulsion)

$Atom_1$–$Atom_2$	A (eV)	ρ (Å)	C (eV Å^6)
Mg–O	1279.69	0.2997	0.00
O–O	9547.96	0.2240	32.0
Al–O	1361.29	0.3013	0.00

Table 2 Comparison of elastic constants, bulk modulus, B, and shear modulus, G, for normal $MgAl_2O_4$ as calculated by DFT and in atomistic simulations with the interactions described by the Ball potential

Prop. (GPa)	Exp. [24]	DFT [21]		MD
		GGA	LDA	
C_{11}	282.5	249	274	405
C_{12}	154.9	140	152	212
C_{44}	154.7	140	159	186
B	197.4	176	193	276
G	109.2	98	110	136

are larger than the experimental values or those determined by DFT; in particular C_{11} is larger by more than 40%, which has a corresponding effect on the bulk modulus. This overestimation does not affect, however, the validity of our study, whose aim is to capture the trends in the thermal and mechanical properties as a function of inversion, rather than to make quantitative predictions. As discussed in the results section, the qualitative trends in the mechanical properties are very well captured, matching the results of the DFT study by Li et al. [21] and another MD study by Chartier et al. [28].

An inverted structure could be created from the normal $MgAl_2O_4$ structure in two different ways: (i) the Al and Mg cations could be directly interchanged or (ii) the Al ions could move to vacant tetrahedral sites while the Mg could move to vacant octahedral sites. The DFT calculations by Gupta [3] showed that direct cation exchange is energetically more favorable. In our simulations, we therefore simply exchanged randomly selected Mg and Al atoms to generate the inverted structures. Since we do not have experimental information on possible ordering in inverted structures, we generated $\sim$7,000 structures for each inversion value via random cation interchange, identified the three lowest energy structures, and used them for our subsequent simulations. The large number of structures for each inversion maximizes our chances of identifying the energetically most favorable structure.

To optimize the structure and determine thermal expansion, we used lattice statics and lattice dynamics at the level of the quasi-harmonic approximation, as implemented in the General Utility Lattice Program (GULP)

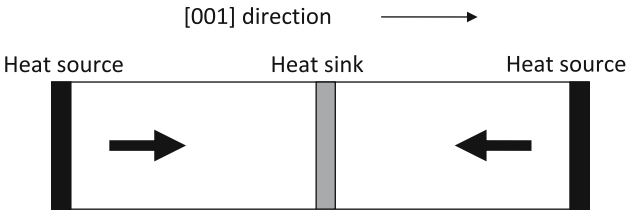

Fig. 2 Schematic of 3-D periodic simulation cell for thermal conductivity simulations

[29, 30]. The thermal conductivity was calculated using MD methods. The thermal conductivity simulations mimic a simple experimental setup with one end in a heat bath and the other in a heat sink. The cooled and heated regions are placed at the center and end of the periodic cell, respectively, thereby setting up two identical heat currents, as illustrated in Fig. 2. This methodology is explained in detail by Schelling et al. [31]. The temperature gradient (∇T) for a given heat current (J) is determined, from which the thermal conductivity (κ) is calculated using Fourier's Law:

$$J = -\kappa \nabla T. \quad (2)$$

Effect of inversion on structure, thermal expansion, and elastic properties

Defects play a major role in materials properties. In the spinel structure, the connectivity of oxygen sublattice remains intact during inversion, though the oxygen ions may displace from their positions in the normal structure. Thus, the cation distribution governs material properties [3]. To investigate the effect of inversion on the cation distribution, we started with the simplest system: one anti-site pair. The Mg ions are larger than the Al ions; thus Al on a tetrahedral (T) sites generates a compressive stress, while Mg on an octahedral (M) site generates a tensile stress. Due to the asymmetry of expansion (M sites) and contraction (T sites) in cation–oxygen bonds, these local stresses have different magnitudes. Figure 3 captures the effect of the spacing between the cations in an anti-site pair on the formation energy for a single anti-site pair. It is evident from Fig. 3 that the anti-sites prefer to be in close proximity. This is physically reasonable since when the anti-sites are close to each other they form a stress dipole, thereby largely compensating each other's strain fields.

Figure 4 shows that the lattice parameter decreases with increasing inversion in a manner similar to that reported by Andreozzi et al. [12]. This increase in density with increasing inversion can be qualitatively understood in terms of a simple picture of the bond strength as a function of bond charge. In normal spinel, a T site is occupied by Mg^{2+} with four O^{2-} neighbors, while an M site is occupied

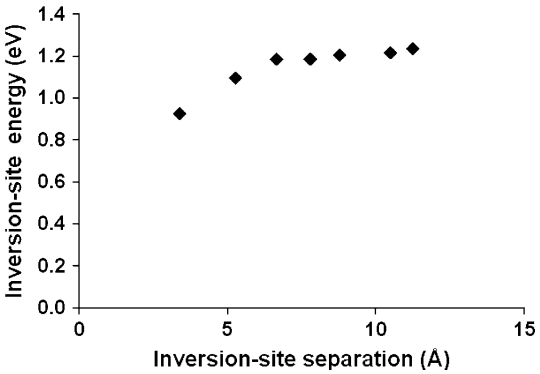

Fig. 3 Formation energy for single anti-site pair as a function of the separation

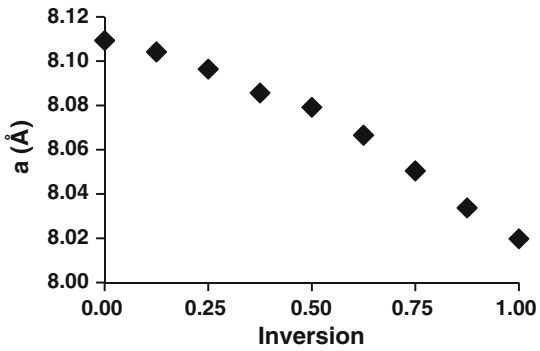

Fig. 4 Effect of inversion on lattice parameter

by Al^{3+} with six O^{2-} neighbors. Each cation shares 1/2 e^- with each neighboring oxygen on both T or M sites. On inversion, Al^{3+} on a T site has four neighboring oxygens, so it shares now 3/4 e^- with each neighboring oxygen, an addition of 1/4 e^- per bond. Similarly, Mg^{2+} on the M site has six neighboring oxygen ions thus sharing 1/3 e^-, a loss of 1/6 e^-, compared to non-inverted spinel. Thus, the decrease in Al–O bond length at T sites is larger than the increase in Mg–O bonds at M sites. This in turn should produce an overall densification of the spinel upon inversion.

The inversion in a sample is mainly controlled by the temperature. Thus, experiment cannot separate the effects of temperature and inversion on material properties (e.g., elastic properties, transition temperature, bond length, and volume). In simulation, however, these two effects can be manipulated independently. Since the experimental data span a narrow range of inversion ($i = 0.16$–0.29), we compared the change in the lattice parameter for the same range of inversion to our MD data. Experimentally the ratio of the $T = 1{,}173$ K, $i = 0.25$ lattice parameter to the $T = 873$ K, $i = 0.18$ is 0.9998 [12]. This suggests that inversion negates the expansion by temperature increase. From Fig. 4 we see that at $T = 0$ K, the $i = 0.25$ system would have a lattice parameter of 99.95% of the $i = 0.18$ system. However, the effects of thermal expansion are such that the ratio of the $T = 1{,}173$ K, $i = 0.25$ lattice parameter to the $T = 873$ K, $i = 0.18$ is 1.0015; thus the contraction associated with inversion (see Fig. 4) and the thermal expansion almost cancel as they did experimentally. This strongly suggests that the simulations are capturing the same fundamental physics as the experiments. Furthermore, the trends observed in experiments [12] and in DFT calculations [18] are similar to those in the MD simulations. As we shall see this densification with inversion affects other physical properties of the system.

Figure 5a shows the cohesive energy of $MgAl_2O_4$ as a function of inversion. Consistent with the normal state being stable, the energy increases with inversion. From this data, it is possible to determine the formation energy for each additional anti-site; this is shown in Fig. 5b. It is evident from Fig. 5b that up to $i \sim 0.375$, the energy required to form new anti-site defects is almost constant. Equivalently, it can be said that at these low inversion levels, existing defects neither make it easier nor harder to form additional anti-site defects. Conversely, beyond $i = 0.375$, it becomes significantly easier to form new defects, with the defect formation energy decreasing by $\sim$25%. This decrease in formation energy can be understood in terms of the effects of the anti-site defects on the local strain. At low inversion, the local strain produced by interchanging Mg and Al cations is small, and is easily relieved, thus not affecting the formation energy for the

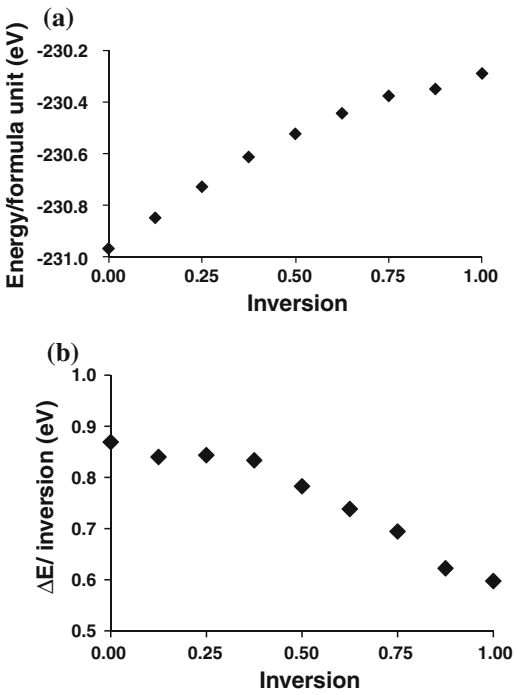

Fig. 5 **a** Cohesive energy as a function of inversion and **b** anti-site formation energy as a function of inversion

next anti-site pair to form. As the inversion increases, however, cation disordering increases and structural relaxation is not able to relieve the strain dipole. Such unrelieved strain dipoles lower the energy required to form strain dipoles of opposite orientation. As a result, the anti-site formation energy actually decreases. This complex effect of inversion is also reflected in the elastic properties.

For a typical solid, the bulk modulus increases as the system becomes denser due to the rapidly increasing interatomic repulsion. Based on this argument, we would expect the bulk modulus to increase monotonically with inversion. As the crosses in Fig. 6 indicate the behavior is actually more complex, the bulk modulus initially decreases slightly, levels off, and then increases rapidly above $i = 0.5$. A similar strong dependence of the bulk modulus at high inversions in $MgAl_2O_4$ was also reported by Chartier et al. in their MD simulations [28].

The volume dependence of the bulk modulus can be understood in terms of the separate contributions of inversion to cation ordering and to volume change. To dissect these effects further, each contribution was studied separately; such a separation is not possible experimentally, but is straightforward in simulation. First, the volume of the system was fixed to that of normal spinel and the bulk modulus was calculated as a function of inversion, thereby picking out the effect of the cation arrangement on bulk modulus (filled circles in Fig. 6). Initially the bulk modulus decreases with inversion, but then it levels off. We already know that inversion causes shortening of Al–O bonds and expanding of Mg–O bonds at inverted sites, respectively. A similar effect of decrease in bulk modulus with cation disordering was experimentally observed in $MgTi_2O_5$ [32]. In the case of single crystal $MgTi_2O_5$, the decrease in bulk modulus was attributed to different compressibilities of weaker Mg–O and stronger Ti–O bonds and the way in which octahedra are arranged. Even though $MgTi_2O_5$ and $MgAl_2O_4$ are structurally different, the behavior of cation disordering are analogous in that they both display weaker Mg–O bonds under cation disordering. Since this is primarily responsible for lowering bulk modulus in $MgTi_2O_5$ for low inversions, it is most likely also related to lowering of bulk modulus in $MgAl_2O_4$. The levelling off of bulk modulus with inversion suggests the limited effect of weak Mg–O bonds in $MgAl_2O_4$, as compared to $MgTi_2O_5$ [32]. This also suggests that there is an increasing effect of Al–O bonds with inversion. Since the shortening of the Al–O bond has precisely the opposite effect, we see a small increase in bulk modulus.

Second, the bulk modulus for normal spinel was calculated as a function of volume (filled triangles in Fig. 6). Using the relationship between the degree of inversion and volume, we can plot the volume dependence of the bulk modulus as a function of inversion to which that volume corresponds (see Fig. 4). It is evident from Fig. 6 that decrease in volume increases the bulk modulus monotonically, consistent with the usual behavior of crystals. To capture the combined effect of volume and cation ordering, the average of these two is taken as an estimate for the dependence of bulk modulus on inversion. As the triangles in Fig. 6 clearly show, this prediction matches the actual simulation results reasonably well. In particular, it shows that the volumetric effect negates the effect of cation disorder essentially up to $i \sim 0.375$. For higher degrees of inversion, further cation disorder has little effect, while the volumetric contraction leads to an increase in the bulk modulus. The other elastic properties were calculated as a function of inversion, with results qualitatively consistent with the DFT calculations by Li et al. [21].

The effect of inversion on thermal expansion is shown in Fig. 7. In a similar manner to the bulk modulus, the thermal expansion is only weakly dependent on inversion up to $i \sim 0.5$, above which it decreases rapidly. In particular, the bulk modulus and the thermal expansion are related through the Grüneisen relation:

$$\alpha = \frac{\gamma C_v}{3B}, \tag{3}$$

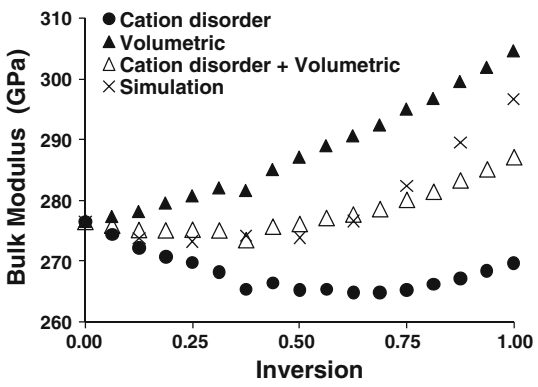

Fig. 6 Bulk modulus as a function of inversion, separating out the volumetric and cation disorder effects

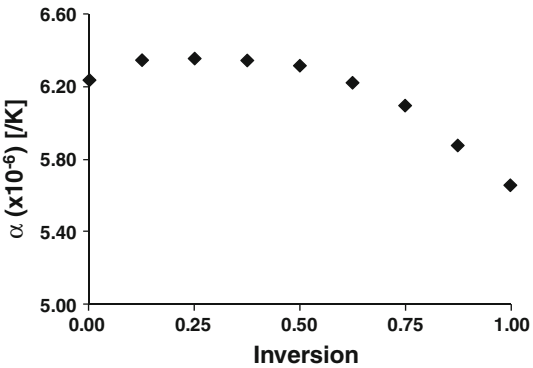

Fig. 7 Coefficient of thermal expansion as a function of inversion

where C_v is the specific heat and γ is the Grüneisen coefficient, which measures the anharmonicity of the interatomic interactions. Using simulated values of α, C_v, and B, γ is calculated using Eq. 3. The dependence of γ on inversion is illustrated in Fig. 8 and suggests that inversion affects γ in the same way as it affects B and α, i.e., it is largely unchanged up to $i \sim 0.5$, above which it changes monotonically. The average value of $\gamma \sim 2$ is consistent with the value of 1.7 reported by Andreozzi et al. [12].

We recall that a key performance metric of a nuclear fuel or inert matrix is a high thermal conductivity. We have thus determined the thermal conductivity of spinel over the full range of inversion, thereby sampling the full range of environments that could be present in a spinel inert matrix over its entire service life in a reactor.

The calculated thermal conductivity can depend quite strongly on the size of the simulation cell by effectively limiting the mean free path of the phonons. To determine the infinite simulation cell size limit of the thermal conductivity, we use the methodology of Schelling et al. [24]. In this method, systems of various lengths in z directions were simulated for thermal conductivity. A careful analysis yields the system size dependence on thermal conductivity, which is given below as Eq. 4.

$$\frac{1}{\kappa} = \frac{1}{\kappa_\infty} + \frac{4P}{L_z}, \tag{4}$$

where κ is the thermal conductivity of system size L_z, κ_∞ is the thermal conductivity in the infinite size limit, and P is a constant. Accordingly, a plot of $1/L_z$ versus $1/\kappa_z$ yields a linear relationship, the intersection to y-axis of the plot gives κ_∞. We performed the system size analysis in our thermal conductivity calculations for all the spinel structures. As Fig. 9 shows in each case the simulation data are well fitted by Eq. 4. The infinite system size extrapolations to $1/L_z = 0$ are taken as our best estimates of the thermal conductivity. The resulting dependence of the calculated thermal conductivity on inversion is shown as diamonds in Fig. 10. The rather weak dependence of the thermal conductivity on inversion is quite surprising when viewed in

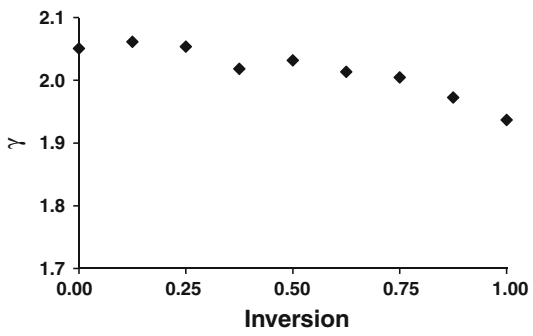

Fig. 8 Dependence of the Grüneisen coefficient on inversion

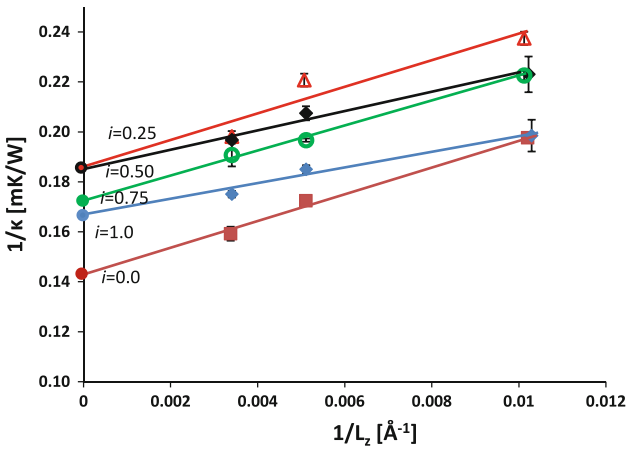

Fig. 9 System size analysis of thermal conductivity for different inversions, intercepts on y-axis are shown as *circles*

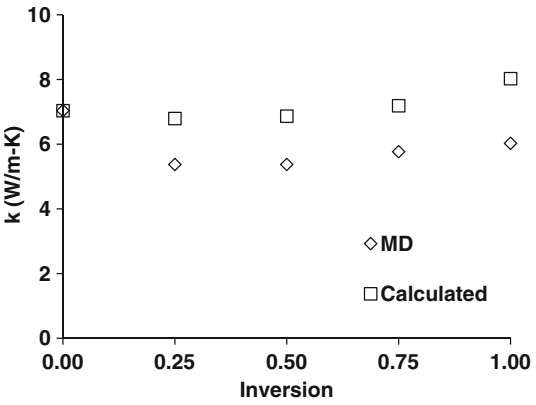

Fig. 10 Dependence of thermal conductivity on inversion

terms of the thermal transport properties of defected ceramics materials. In particular both experiments and MD simulations of fluorite structure materials (e.g., yttria-doped zirconia and hyperstoichiometric UO_2) have shown a strong decrease in thermal conductivity with even quite low defect concentrations [33]. The key difference between the spinel case and the fluorite structured materials is that here disorder only involves anti-site defects, while for the fluorites the disorder involved oxygen vacancies (zirconia) and oxygen interstitials (urania), which presumably affect the phonon properties and hence thermal conductivity much more strongly.

We can understand this inversion dependence in a quantitative manner, by recalling that the thermal conductivity is given by [34]:

$$\kappa \sim \frac{24}{10}\frac{(4)^{1/3}}{\gamma^2}\left(\frac{k_B}{h}\right)^3 Ma\frac{\Theta^3}{T}. \tag{5}$$

Here, k_B and h are Boltzmann and Planck constants, a^3 is the volume, M is mass per atom, and Θ is the Debye temperature. Equation 5 is based on the Debye

approximation, which assumes every phonon mode present in the system is acoustic and contributes to the thermal conductivity. It fairly well captures the picture for very simple systems but as the structural complexity increases, the actual thermal conductivity values deviate from the predicted values. For our system, even though Eq. 5 cannot be expected to quantitatively predict the thermal conductivity, it still should still capture the qualitative picture of how thermal conductivity changes with inversion. In Eq. 6, the Grüneisen parameter (γ), lattice parameter (a), and Θ may all vary with inversion. The dependence on inversion of γ and a were discussed above. The dependence of the Debye temperature on inversion arises from the changes in the density, ρ, B, and shear modulus (G) and can be determined from

$$\Theta = \frac{h}{2\pi k}\left(\frac{6\pi^2}{V_{\text{at}}}\right)^{1/3}\left(\frac{1}{3}\left(\frac{3B+4G}{3\rho}\right)^{-3/2}+\frac{2}{3}\left(\frac{G}{\rho}\right)^{-3/2}\right)^{-1/3}, \tag{6}$$

Together, a, γ, and Θ are used to calculate the dependence of κ on inversion. Proportionality constant in Eq. 5 is calculated by normalizing κ for $i = 0$ to value determined from the simulation; the same proportionality constant is used for the thermal conductivity at all inversion values in Fig. 10.

As Fig. 10 shows the dependence of the thermal conductivity on inversion determined directly from the MD simulations and from Eq. 5 are in reasonably good agreement. Our trust in the qualitative picture offered by MD is strengthened by the fact that the value of $\kappa \sim 13$ W/m K at 500 K by MD compares very well with experimental result of $\sim$15 W/m K of Burghartz [22]. In particular, the simulated and calculated values both predict that the thermal conductivity of the fully inverted system should be very similar to that of the normal spinel structure [22].

The thermal conductivity calculated from MD does show a shallow minimum at $i \sim 0.5$, not predicted from the anharmonicity analysis alone. Since inversion leads to volume change and cation disorder, it is necessary to probe both to understand this unusual behavior. To capture the volume effect in isolation, we kept the volume constant at the $i = 0.0$ value and generated structures for inversions of $i = 0.5$ and $i = 1.0$. Similarly, we generated a normal structure with the lattice parameter of $i = 1.0$. The thermal conductivity values are plotted in Fig. 11 and compared with simulated values from Fig. 10. The data points essentially overlap, indicating that the effect of density on the thermal conductivity is negligible. To capture the effect of cation arrangement on thermal conductivity, approximately 7,000 different structures with random arrangements of cations were generated for each value of inversion. The thermal conductivities were calculated for

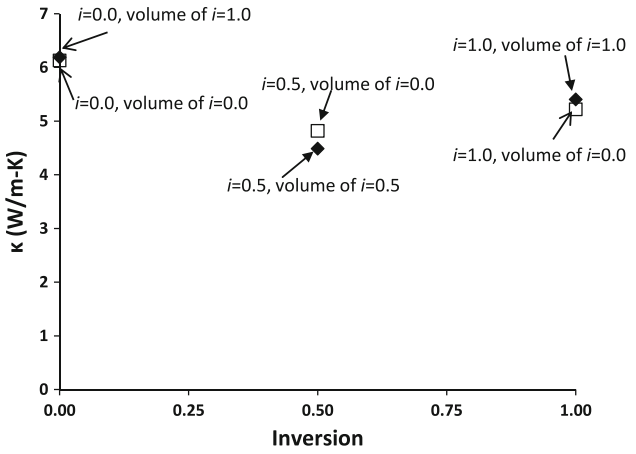

Fig. 11 Density effect on thermal conductivity for $i = 0.0$, 0.50, and 1.0

three different structures: the lowest energy structure, the highest energy structure, and one structure with an intermediate energy. The variation in the thermal conductivity values between these three structures was <1%. This shows that the degree of inversion affects the thermal conductivity, but the precise atomic arrangements do not.

The minimum in thermal conductivity as a function of inversion can be attributed to the degree of disorder in the system which, for the fluorites, led to a significant drop in the thermal conductivity [35–37]. This disorder can be characterized by the number of different configurations of the defects in the lattice. For example, for $i = 0$, Mg and Al occupy tetrahedral and octahedral positions and there is only one way to arrange the cations. For one anti-site pair, in one unit cell system, one Mg can be in any of the 16 possible Al sites and also Mg can be chosen in eight different ways. The multiplicity of these possible arrangements with inversion can be expected to have an impact on thermal conductivity. Figure 12 captures the variation of the number of possible arrangement for each cation site with inversion. As we can see, there is a maximum in the number of different defect arrangements at $i = 0.67$, at which point the system would display the maximum number of different scattering environments. If there were no other effects, we would thus expect this to result in a minimum in the thermal conductivity at $i = 0.67$. The thermal conductivity is actually a minimum at close to $i = 0.5$ suggests that the disorder on the A sublattice actually affects the phonon scattering more strongly than the disorder on the B site. This can be understood in terms of local strain produced at inverted sites. As previously discussed, the T_{Al} sites experience greater strain than the M_{Mg} sites and thus affect material properties to a greater extent. As inversion increases, T_{Al} experiences more chemical disorder; at $i = 0.5$ half are occupied by Mg and half by Al; above $i = 0.5$ they become more and more populated by Al ions.

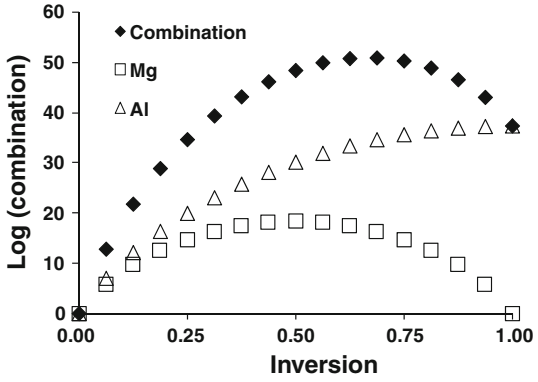

Fig. 12 Combinatoric analysis of the number of distinct Mg–Al exchanges possible in 2 × 2 × 2 unit cell as a function of inversion

Conclusions

In this work, we have investigated the effect of inversion on the lattice parameter, elastic properties, and thermal properties of $MgAl_2O_4$ by atomic-level simulations. The decrease in volume with increasing inversion was consistent with experimental findings. We observed that the anti-site formation energy is constant up to $i \sim 0.5$. This was also reflected in the small change of bulk modulus and thermal expansion coefficient up to $i \sim 0.5$. The anharominicity in the interatomic interactions was calculated from the thermal expansion coefficient and bulk modulus, and was found to be only weakly dependent on the inversion. This also led to the very weak dependence of the thermal conductivity on inversion. Small decreases in the thermal conductivity for intermediate values of inversion were attributed to phonon scattering from the anti-site defects. It was also found that the Al–O bonds at inverted sites affected material properties to a greater degree than Mg–O bonds. The near invariance in thermal conductivity as a function of inversion is particularly significant for nuclear application, since it means that the thermal conductivity will remain essentially fixed under all realistic radiation and storage conditions.

Acknowledgements We are happy to acknowledge the University of Florida High-Performance Computing Center for providing computational resources and support that have contributed significantly to the research results reported in this article. This work was funded by DOE-NERI Award DE-FC07-05ID14647 and by a Materials World Network Project, NSF DMR-0710523.

References

1. Glasso FS (1970) Structure and properties of inorganic solids. Pergamon, New York
2. Ueda N et al (1992) Appl Phys Lett 61:1954
3. Gupta RP (2006) J Nucl Mater 358:35
4. Matzke H et al (1999) J Nucl Mater 274:47
5. Wiss T, Matzke H (1999) Radiat Meas 31:507
6. Buckley SN (1986) J Nucl Mater 141:387
7. Buckley SN, Shaibani SJ (1987) Philos Mag Lett 55:15
8. Sickafus KE et al (1995) J Nucl Mater 219:128
9. Bordes N et al (1995) J Nucl Mater 225:318
10. Ball JA et al (2005) J Phys Condens Matter 17:7621
11. Sickafus KE et al (1999) J Am Ceram Soc 82:3279
12. Andreozzi GB et al (2000) Am Mineral 85:1164
13. Schmocker U et al (1972) Phys Lett A 40:237
14. Schmocker U, Waldner F (1976) J Phys Condens Matter 9:L235
15. Goodenough JB, Loeb AL (1955) Phys Rev 98:391
16. Suzuki I et al (2000) Am Mineral 85:304
17. Suzuki I, Kumazawa M (1980) Phys Chem Miner 5:279
18. Seko A et al (2006) Phys Rev B 73:184117
19. Lavrentiev MY et al (2003) Am Mineral 88:1522
20. Thibaudeau P et al (2006) Phys Rev B 73:064305
21. Li L et al (2007) Am Mineral 92:174
22. Burghartz S, Schulz B (1994) J Nucl Mater 215:1065
23. Catlow CRA et al (1977) J Phys Condens Matter 10:1395
24. Schelling PK et al (2002) Phys Rev B 65:144306
25. Chang ZP, Barsch GR (1973) J Geophys Res 78:2418
26. Cynn H et al (1993) Pure Appl Geophys 141:415
27. Yoneda A (1990) J Phys Earth 38:19
28. Chartier A et al (2008) J Nucl Mater 378:188
29. Gale JD, Rohl AL (2003) Mol Simul 29:291
30. Gale JD (1997) J Chem Soc Faraday Trans 93:629
31. Schelling PK, Phillpot SR (2001) J Am Ceram Soc 84:2997
32. Hazen RM, Yang HX (1997) Science 277:1965
33. Watanabe T et al (2009) J Am Ceram Soc 92:850
34. Leibfried G, Schloemann E (1954) Akad Wiss Goettingen Math-Physik 4:71
35. Raghavan S et al (1998) Scr Mater 39:1119
36. Bisson JF et al (2000) J Am Ceram Soc 83:1993
37. Leclercq B et al (2003) Mat-wiss Werkstofftech 34:406